

STARS: Self-supervised Tuning for 3D Action Recognition in Skeleton Sequences

Soroush Mehraban^{1,2,3}, Mohammad Javad Rajabi^{1,2}, Andrea Iaboni^{1,3}, Babak Taati^{1,2,3}

¹University of Toronto ²Vector Institute ³KITE Research Institute, UHN

Project Page: <https://soroushmehraban.github.io/stars/>

Abstract

Self-supervised pretraining methods with masked prediction demonstrate remarkable within-dataset performance in skeleton-based action recognition. However, we show that, unlike contrastive learning approaches, they do not produce well-separated clusters. Additionally, these methods struggle with generalization in few-shot settings. To address these issues, we propose Self-supervised Tuning for 3D Action Recognition in Skeleton sequences (STARS). Specifically, STARS first uses a masked prediction stage using an encoder-decoder architecture. It then employs nearest-neighbor contrastive learning to partially tune the weights of the encoder, enhancing the formation of semantic clusters for different actions. By tuning the encoder for a few epochs, and without using hand-crafted data augmentations, STARS achieves state-of-the-art self-supervised results in various benchmarks, including NTU-60, NTU-120, and PKU-MMD. In addition, STARS exhibits significantly better results than masked prediction models in few-shot settings, where the model has not seen the actions throughout pretraining.

1. Introduction

Human action recognition is receiving growing attention in computer vision due to its wide applications in the real world, such as security, human-machine interaction, medical assistance, and virtual reality [22, 34, 46, 49]. While some previous works have focused on recognizing actions based on appearance information, other approaches have highlighted the benefits of using pose information. In comparison to RGB videos, Representing videos of human activities with 3D skeleton sequences offers advantages in privacy preservation, data efficiency, and excluding extraneous details such as background, lighting variations, or diverse clothing types. Recent models for 3D action recognition based on skeleton sequences have demonstrated impressive results [7, 12, 13, 23]. However, these models heavily depend on annotations, which are labor-intensive and time-consuming to acquire. Motivated by this, in this study, we

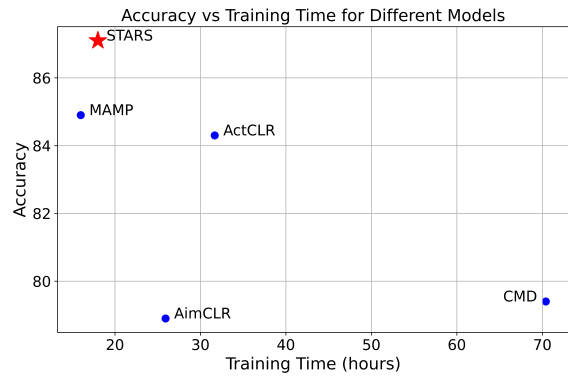


Figure 1. Comparison between training time and test-time accuracy on linear evaluation protocol. Training time is evaluated on a single NVIDIA GeForce RTX 3090 GPU.

investigate the self-supervised representation learning of 3D actions.

Prior studies in self-supervised learning have employed diverse pretext tasks, such as predicting motion and recognizing jigsaw puzzles [26, 40, 54]. More recently, current research has shifted its focus towards contrastive learning [27, 30, 32] or Mask Autoencoders (MAE) [31, 47].

Contrastive learning approaches, although effective in learning representations, rely heavily on data augmentations to avoid focusing on spurious features. Without using data augmentations, they are prone to the problem of shortcut learning [16], leading to potential overfitting on extraneous features, such as a person’s height or the camera angle, which do not provide a valid cue to discriminate between different actions. As a result, some knowledge expert [44] is needed to design different augmentations of the same sequence; and methods that incorporate extreme augmentations in their pretraining pipeline [18, 27] have shown significant improvements.

MAE-based methods mask out a proportion of the input sequence and use an encoder-decoder architecture to reconstruct the missing information from the input based on the latent representation of unmasked regions. These approaches [31, 47] have recently outperformed their con-

trastive counterparts in within-dataset metrics. However, we show that representations learned by these models cannot separate different actions as effectively as contrastive learning-based methods in few-shot settings.

Despite the significant efforts that have been made, how to learn a more discriminative representation of skeletons is still an issue for skeleton-based action recognition. MAE methods emphasize high-frequency details, while contrastive learning (CL) focuses on global semantics and low-frequency information [35]. Combining them can improve generalizability while preserving the strong within-dataset performance of MAE models. To this end, we propose Self-supervised Tuning for 3D Action Recognition in Skeleton S

In summary, our main contributions are as follows:

- We propose the STARS framework, a sequential approach that improves the MAE encoder output representation to create well-separated clusters, without any extra data augmentations, and with only a few epochs of contrastive tuning.
- We show that, although MAE approaches excel in within-dataset evaluations, they exhibit a lack of generalizability in few-shot settings. Subsequently, we significantly enhance their few-shot capabilities while maintaining their strong within-dataset performance by employing our method.
- We validate the efficacy of our approach through extensive experiments and ablations on three large datasets for 3D skeleton-based action recognition, attaining state-of-the-art performance in most cases.

2. Related Works

2.1. Self-supervised Skeleton-Based Action Recognition

The objective of self-supervised action recognition is to train an encoder to discriminate sequences with different actions without providing any labels throughout the training. Methods such as LongTGAN [54] pretrain their model with 3D skeleton reconstruction using an encoder-decoder architecture; and P&C [40] improves the performance by employing a weak decoder. Colorization [50] represents the sequence as 3D point clouds and colorizes it based on the

temporal and spatial orders in the original sequence.

Several studies explored various contrastive learning approaches, showing promising results [18, 25, 27, 30, 32]. CrosSCLR [25] applies the MoCo [19] framework and introduces cross-view contrastive learning. This approach aims to compel the model to maintain consistent decision-making across different views. AimCLR [18] improves the representation by proposing extreme augmentations. CMD [30] trains three encoders simultaneously and distills knowledge from one to another by introducing a new loss function. I²MD [32] extends the CMD framework by introducing intra-modal mutual distillation, aiming to elevate its performance through incorporating local cluster-level contrasting. ActCLR [27] employs an unsupervised approach to identify actionlets, which are specific body areas involved in performing actions. The method distinguishes between actionlet and non-actionlet regions and applies more severe augmentations to non-actionlet regions.

Recently, MAE-based approaches showed significant improvements. SkeletonMAE [47] reconstructs the spatial positions of masked tokens. MAMP [31] uses temporal motion as its reconstruction target and proposes a motion-aware masking strategy. However, we show that MAE-based methods exhibit limited generalization in few-shot settings when compared to contrastive-learning based approaches.

2.2. Combining Masked Autoencoders with Instance Discrimination

Some recent works in the image domain investigated the effect of combining MAE and Instance Discrimination (ID) methods [24, 33, 42, 45, 55]. iBOT [55] combines DINO [6] and BEiT [4] for the pretext task. RePre [45] extends the contrastive learning framework by adding pixel-level reconstruction loss. CAN [33] adds gaussian noise to the unmasked patches and it reconstructs the noise and masked patches, and adds a contrastive loss to the encoder output. MSN [3] aligns an image view featuring randomly masked patches with the corresponding unmasked image. SiameseIM [42] predicts dense representations from masked images in different views. MAE-CT [24] proposes a sequential training by adding contrastive loss after MAE training.

Our work is a sequential self-supervised approach for pretraining of skeleton sequences. It initially employs an MAE approach using an encoder-decoder architecture and further enhances the output representation of the encoder by tuning its weights using contrastive learning.

3. Method

3.1. Framework Overview

The overall framework of STARS is illustrated in Fig. 2. It is a sequential self-supervised approach consisting of

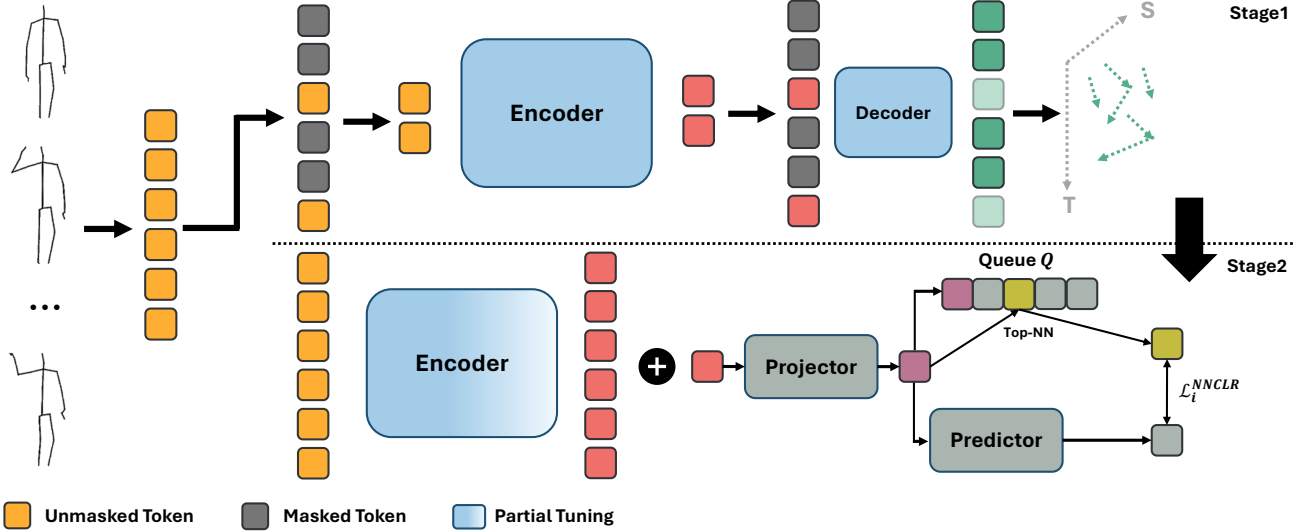


Figure 2. The overall pipeline of our proposed STARS framework. The first stage uses MAMP [31] to reconstruct the motion of masked tokens. The second stage trains parameters of the projector and predictor using a contrastive learning approach in addition to partially tuning the encoder weights.

two main stages. The first stage relies on an MAE-like framework to pretrain the weights of the encoder. We use MAMP [31] because it shows promising result in 3D action representation learning; however, any alternative MAE-based approach is also applicable. The next stage is designed to tune the parameters of the encoder using an instance discrimination method. Specifically, the second stage replaces the decoder with a projector and predictor [17]. It trains them in addition to the encoder using Nearest-Neighbor Contrastive Learning (NNCLR) [14] to converge to a representation capable of discriminating different sequences. This approach helps the encoder learn to output distinct clusters for different actions, improving its ability to discriminate between various sequences.

3.2. MAMP Pre-training (Stage 1)

MAMP [31] uses a transformer encoder-decoder architecture to reconstruct motions from the 3D skeleton sequence. It receives the input skeleton sequence $\mathbf{S} \in \mathbb{R}^{T_s \times V \times C_s}$, where T_s , V , and C_s are the temporal length, number of joints, and coordinate channels, respectively. Next, the sequence is divided into non-overlapping segments $\mathbf{S}' \in \mathbb{R}^{T_e \times V \times l \cdot C_s}$, where $T_e = T_s/l$ and l is the segment length. This division results in having $T_e \times V$ tokens and reduces the temporal resolution by a factor of l . Subsequently, the input joints are linearly projected into joint embedding $\mathbf{E} \in \mathbb{R}^{T_e \times V \times C_e}$ where C_e is the dimension of embedding features.

As for the pretraining objective and the masking strategy, MAMP leverages the motion information. Given an origi-

nal sequence \mathbf{S} , the motion $\mathbf{M} \in \mathbb{R}^{T_s \times V \times C_s}$ is derived by employing temporal difference on joint coordinates:

$$\mathbf{M}_{i,:,:} = \mathbf{S}_{i,:,:} - \mathbf{S}_{i-m,:,:}, \quad i \in m, m+1, \dots, T_s-1 \quad (1)$$

where the step size of the motion is controlled by the hyperparameter m . Specifically, MAMP uses a stride of $m = l$ to capture motion among different segments of the sequence.

For masking the input sequence based on the motion, the obtained motion \mathbf{M} should have the same dimension as the segmented sequence \mathbf{S}' . Hence, the motion \mathbf{M} is padded by replicating the sequence and further reshaped into $\mathbf{M}' \in \mathbb{R}^{T_e \times V \times l \times C_s}$. Subsequently, to signify the importance of motion in each spatio-temporal segment, the motion intensity \mathbf{I} is calculated as follows:

$$\mathbf{I} = \sum_{i=0}^l \sum_{j=0}^{C_i} |\mathbf{M}'_{i,:,:j}| \in \mathbb{R}^{T_e \times V}, \quad (2)$$

$$\mathbf{P} = \text{Softmax}(\mathbf{I}/\tau_1),$$

where \mathbf{P} indicates the probability of masking each embedding feature, and τ_1 is a temperature hyperparameter. Finally, to increase the diversity in mask selection, the Gumbel-Max trick is used:

$$\mathbf{G} = -\log(-\log \epsilon), \quad \epsilon \in U[0, 1]^{T_e \times V}, \quad (3)$$

$$idx^{\text{mask}} = \text{Index-of-Top-K}(\log \mathbf{P} + \mathbf{G}),$$

where $U[0, 1]$ represents a uniform distribution ranging from 0 to 1, and idx^{mask} denotes the masked indices.

On the joint embedding \mathbf{E} , spatio-temporal positional embedding is added and unmasked tokens are passed to the encoder. Following the computation of the encoder's latent representations, learnable mask tokens are inserted to them according to the mask indices idx^{mask} . The decoder then predicts the motion M^{pred} and the reconstruction loss is computed by applying mean squared error (MSE) between the predicted motion \mathbf{M}^{pred} and the reconstruction target $\mathbf{M}^{\text{target}}$, as follows:

$$\mathcal{L} = \frac{1}{|idx^{\text{mask}}|} \sum_{(i,j) \in idx^{\text{mask}}} \|(\mathbf{M}_{i,j,:}^{\text{pred}} - \mathbf{M}_{i,j,:}^{\text{target}})\|_2^2. \quad (4)$$

3.3. Contrastive tuning (Stage 2)

In the second stage, we replace the decoder with projection and prediction modules. The projection module aligns the encoder representation with a space targeted for contrastive loss. The prediction module takes one positive sample from a pair and generates a representation vector resembling the other sample in the positive pair to minimize the contrastive loss. More specifically, The encoder f_θ receives segmented sequence tokens \mathbf{S}' and outputs representation tokens $\mathbf{Y}_\theta = f_\theta(\mathbf{S}')$. After applying average pooling of the output tokens, the projector g_θ aligns the result to the final representation vector $\mathbf{z}_\theta = g_\theta(\bar{\mathbf{Y}}_\theta)$. Following the NNCLR approach, vector \mathbf{z}_θ is inserted into the queue Q and is compared to sequence representations from previous iterations. From these representations, the top nearest neighbor is sampled as a positive sample in contrastive loss:

$$\text{NN}(\mathbf{z}, Q) = \arg \min_{q \in Q} \|\mathbf{z} - \mathbf{q}\|_2 \quad (5)$$

Concurrently, the feature vector \mathbf{z}_θ is given to predictor module to output the feature \mathbf{z}_θ^+ . Next, given positive pairs $(\text{NN}(\mathbf{z}, Q), \mathbf{z}^+)$, we have:

$$\mathcal{L}_i^{\text{NNCLR}} = -\log \frac{\exp(\text{NN}(\mathbf{z}_i, Q) \cdot \mathbf{z}_i^+ / \tau_2)}{\sum_{k=1}^n \exp(\text{NN}(\mathbf{z}_i, Q) \cdot \mathbf{z}_k^+ / \tau_2)} \quad (6)$$

where τ_2 is a fixed temperature hyperparameter, i is the sample index in batch of data, and n is the batch size. Notably, in contrast to other contrastive learning approaches, our method operates more effectively with a single, unaltered view of the sequence, without relying on two different augmented views. Additionally, we show (later, in Fig. 3) that after training these two modules, the predictor output representation forms better cluster separation compared to the encoder trained with MAMP framework in previous stage.

In addition to projector and predictor modules, we partially tune the encoder parameters to produce well-separated

clusters. Specifically, we use layer-wise learning rate decay [9] to tune the second-half of the encoder parameters. This is formulated as:

$$LR_i = \text{BaseLR} * \alpha^{(N-i)} \quad (7)$$

where LR_i denotes learning rate of the i^{th} layer, α is the learning rate decay, and N is the total number of layers.

4. Experiments

4.1. Datasets

NTU-RGB+D 60 [38] is a large-scale dataset containing 56,880 3D skeleton sequences of 40 subjects performing 60 actions. In this study, we use the recommended cross-subject (X-sub) and cross-view (X-view) evaluation protocols. In the cross-subject scenario, half of the subjects are selected for the training set, and the remaining subjects are used for testing. For the cross-view evaluation, sequences captured by cameras 2 and 3 are employed for training, while camera 1 sequences are used for testing.

NTU-RGB+D 120 [29] is the extended version of NTU-60, in which 106 subjects perform 120 actions in 114,480 skeleton sequences. The authors also substitute the cross-view evaluation protocol with cross-setup (X-set), where sequences are divided into 32 setups based on camera distance and background. Samples from half of these setups are selected for training and the rest for testing.

PKU-MMD [28] contains around 20,000 skeleton sequences of 52 actions. We follow the cross-subject protocol, where the training and testing sets are split based on subject ID. The dataset contains two phases: PKU-I and PKU-II. The latter is more challenging because of more noise introduced by larger view variations, with 5,332 sequences for training and 1,613 for testing.

4.2. Experimental Setup

Data Preprocessing: From an initial skeleton sequence, a consecutive segment is randomly trimmed with a proportion p , where p is sampled from the range $[0.5, 1]$ during training and, similar to [31], remains fixed at 0.9 during testing. Subsequently, the segment is resized to a consistent length T_s using bilinear interpolation. By default, T_s is set to 120.

Network Architecture: We adopted the same network architecture as MAMP [31]. It uses a vanilla vision transformer (ViT) [11] as the backbone with $L_e = 8$ transformer blocks and temporal patch size of 4. In each block, the embedding dimension is 256, number of multi-head attentions is 8, and hidden dimension of the feed-forward network is 1024. It also incorporates two spatial and temporal positional embeddings into the embedded inputs. The decoder used in first stage is similar to the transformer encoder except that it has $L_d = 5$ layers. In the contrastive tuning

Method	Input	NTU-60		NTU-120		PKU-I XSub(%)	PKU-II XSub(%)
		XSub(%)	XView(%)	XSub(%)	XSet(%)		
<i>Other pretext tasks:</i>							
LongTGAN [54]	Single-stream	39.1	48.1	-	-	67.7	26.0
<i>Contrastive Learning:</i>							
ISC [43]	Single-stream	76.3	85.2	67.1	67.9	82.8	36.0
CrosSCLR [25]	Three-stream	77.8	83.4	67.9	66.7	84.9	21.2
AimCLR [18]	Three-stream	78.9	83.8	68.2	68.8	87.4	39.5
CPM [51]	Single-stream	78.7	84.9	68.7	69.6	88.8	48.3
PSTL [56]	Three-stream	79.1	83.8	69.2	70.3	89.2	52.3
CMD [30]	Single-stream	79.4	86.9	70.3	71.5	-	43.0
HaLP [37]	Single-stream	79.7	86.8	71.1	72.2	-	43.5
HiCLR [52]	Three-stream	80.4	85.5	70.0	70.4	-	-
HiCo-Transformer [10]	Single-stream	81.1	88.6	72.8	74.1	89.3	49.4
SkeAttnCLR [20]	Three-stream	82.0	86.5	77.1	80.0	89.5	55.5
I ² MD [32]	Three-stream	83.4	88.0	73.1	74.1	-	49.0
ActCLR [27]	Three-stream	84.3	88.8	74.3	75.7	-	-
UmURL [41]	Single-stream	82.3	89.8	73.5	74.3	-	52.1
<i>Masked Prediction:</i>							
SkeletonMAE [47]	Single-stream	74.8	77.7	72.5	73.5	82.8	36.1
MAMP [31]	Single-stream	84.9	89.1	78.6	79.1	<u>91.9*</u>	52.0*
S-JEPA [1]	Single-stream	85.3	89.8	79.6	79.9	92.2	53.5
<i>Masked Prediction + Contrastive Learning:</i>							
PCM ³ [53]	Single-stream	83.9	90.4	76.5	77.5	-	51.5
STARS-3stage (Ours)	Single-stream	<u>86.3</u>	<u>90.7</u>	<u>79.3</u>	<u>80.6</u>	91.5	52.2
STARS (Ours)	Single-stream	87.1	90.9	79.9	80.8	91.2	52.7

Table 1. Performance comparison on NTU-60, NTU-120, and PKU-MMD in the linear evaluation protocol. *Single-stream*: Joint. *Three-stream*: Joint+Bone+Motion. The best and second-best accuracies are in bold and underlined, respectively. * indicates that result is reproduced using our GPUs.

Method	NTU 60		NTU 120	
	XSub(%)	XView(%)	XSub(%)	XSet(%)
P&C [40]	50.7	75.3	42.7	41.7
ISC [43]	62.5	82.6	50.6	52.3
MAMP [31]	63.1	80.3	51.8	56.1
CrosSCLR-B [25]	66.1	81.3	52.5	54.9
CMD [30]	70.6	85.4	58.3	60.9
I ² MD [32]	75.9	83.8	62.0	64.7
STARS-3Stage (Ours)	<u>76.9</u>	<u>88.0</u>	<u>65.7</u>	68.0
STARS (Ours)	79.9	88.6	67.6	<u>67.7</u>

Table 2. Performance comparison on NTU-60 and NTU-120 in the KNN evaluation protocol (K=1).

modules used in the second stage, the projector module is solely a Batch Normalization [21], given the relatively small size of the 256-dimensional embedding space. The predictor module consists of a feed-forward network with a single hidden layer sized at 4096.

Pre-training: The first stage follows the same setting as

MAMP [31]. For the second stage, we use the AdamW optimizer with weight decay 0.01, betas (0.9, 0.95), and learning rate 0.001. In the second stage, we train the projection and prediction modules in addition to finetuning the encoder for 20 epochs, and the best representation is chosen based on K-NN (K=10) on validation data. We employ layer-wise learning rate decay with a decay rate of 0.20. All the pre-training experiments are conducted using PyTorch on four NVIDIA A40 GPUs with a batch size of 32 per GPU.

4.3. Evaluation and Comparison

In all evaluation protocols, we report on STARS, the method proposed in section 3, as well as STARS-3stage. STARS-3stage involves a three-stage pretraining process. The second stage is divided into two parts: the Head Initialization stage, where only the projector and predictors are trained, and the contrastive tuning stage, where the encoder is finetuned along with the head modules. More details can be found in the supplementary materials.

Linear Evaluation Protocol: In this protocol, the weights of the pretrained backbone are frozen and a linear classifier is trained with supervision to evaluate the linear-separability of the learned features. We train the linear classifier for 100 epochs with a batch size of 256 and a learning rate of 0.1, which is decreased to 0 by a cosine decay schedule. We evaluate the performance on the NTU-60, NTU-120, and PKU-II datasets. As shown in Tab. 1, our proposed STARS outperforms other methods on both NTU benchmarks. On the PKU-II dataset, STARS achieves second-best result, and SkeAttnCLR [20] outperforms it using a three-stream input method.

KNN Evaluation Protocol: An alternative way to evaluate the pretrained encoder is by directly applying a K-Nearest Neighbor (KNN) classifier to their output features. Following other works [30, 32, 40], each test sequence is compared to all training sequences using cosine similarity and the test prediction is based on the label of the most similar neighbor (i.e. KNN with $k=1$). Tab. 2 compares different methods using KNN evaluation protocol. Notably, we find that MAMP cannot achieve competitive results compared to contrastive learning models, despite showing superior results on linear evaluation. We believe that this is because of the pretraining objective of contrastive learning models, which, by pushing different samples into different areas of the representation space, results in better-separated clusters. Our STARS approach leverages contrastive tuning to enhance the feature representation of MAMP, outperforming all other methods. This demonstrates the superiority of contrastive tuning over contrastive learning approaches.

Fine-tuned Evaluation Protocol: We follow MAMP and by adding MLP head on the pretrained backbone, the whole network is fine-tuned for 100 epochs with batch size of 48. The learning rate starts at 0 and is gradually raised to $3e-4$ during the initial 5 warm-up epochs, after which it is reduced to $1e-5$ using a cosine decay schedule. As shown in Tab. 3, both MAMP and STARS notably enhance the performance of their transformer encoder without pretraining. However, these results indicate that contrastive tuning following MAMP pretraining does not impact the fine-tune evaluation, and MAMP and STARS achieve nearly identical results, both outperforming other approaches.

Transfer Learning Protocol: In this protocol, the transferability of the learned representation is evaluated. Specifically, the encoder undergoes pretraining on a source dataset using a self-supervised approach, followed by fine-tuning on a target dataset through a supervised method. In this study, NTU-60 and NTU-120 are selected as the source datasets, with PKU-II chosen as the target dataset. Tab. 4 shows that when fine-tuned on a new dataset, masked prediction techniques like SkeletonMAE and MAMP demonstrate superior transferability compared to contrastive learning methods. Moreover, STARS enhances performance

when pre-trained on NTU-60, but its effectiveness diminishes when pre-trained on NTU-120.

Few-shot Evaluation Protocol: This protocol evaluates the scenario where only a small number of samples are labeled in the target dataset. This is crucial in practical applications like education, sports, and healthcare, where actions may not be clearly defined in publicly available datasets. In this protocol, we pretrain the model on NTU-60 (XSub) and evaluate it on the evaluation set of 60 novel actions on NTU-120 (XSub) using n labeled sequences for each class in n -shot setting. For the evaluation, we follow MotionBERT [57] and calculate the cosine distance between the test sequences and the exemplars, and use n -nearest neighbors to determine the action. Tab. 5 compares different methods in the few-shot settings. Notably, MAMP demonstrates poor generalization performance, in contrast to its robust performance in transfer learning and evaluations within the dataset. By applying contrastive tuning, STARS surpasses contrastive learning approaches in all settings, demonstrating its strength in various evaluations.

Qualitative Comparison: Fig. 3 compares the t-SNE visualization of our proposed STARS method with AimCLR [18], CMD [30], HiCo-Transformer [10], and MAMP [31]. CMD adds cross-modal mutual distillation loss to contrastive learning and by ensuring that various input modalities (joint, bone, and motion) exhibit the same neighborhood, it scatters actions across different areas of space and mitigates the impact of applying contrastive learning loss. On the other hand, AimCLR and HiCo-Transformer create distinct clusters through the use of extreme augmentations and by applying contrastive loss at different hierarchical levels, respectively. When compared to MAMP, these two contrastive learning methods exhibit a higher inter-cluster distance than MAMP. Interestingly, actions involving interactions between two individuals, such as kicking, giving objects, and shaking hands, create a distinct higher-level cluster compared to actions involving a single person across various methods. Specifically, MAMP shows the highest distance between these two cluster groups, whereas within each group, the action clusters are closely situated. By employing contrastive tuning, STARS effectively minimizes intra-cluster distance (as seen in examples like sneeze/cough) while maximizing inter-cluster distance. This leads to the formation of clearly separated clusters, each representative of different actions.

4.4. Ablation Study

Tuning Strategy Design: Tab. 6 compares the NNCLR strategy used in our STARS framework with DINO and MoCo. DINO [6] employs a student-teacher framework. It updates the student’s weights by relying on the teacher’s output, which is constructed using a momentum encoder, as the target. Unlike contrastive learning methods, DINO does

Method	Input	Backbone	NTU 60		NTU 120	
			XSub(%)	XView(%)	XSub(%)	XSet(%)
<i>Other pretext tasks:</i>						
Colorization [50]	Three-stream	DGCNN	88.0	94.9	-	-
Hi-TRS [8]	Three-stream	Transformer	90.0	95.7	85.3	<u>87.4</u>
<i>Contrastive Learning:</i>						
CPM [51]	Single-stream	ST-GCN	84.8	91.1	78.4	78.9
CrosSCLR [25]	Three-stream	ST-GCN	86.2	92.5	80.5	80.4
I ² MD [32]	Single-stream	GCN-TF*	86.5	93.6	79.1	80.3
AimCLR [18]	Three-stream	ST-GCN	86.9	92.8	80.1	80.9
ActCLR [27]	Three-stream	ST-GCN	88.2	93.9	82.1	84.6
HYSP [15]	Three-stream	ST-GCN	89.1	95.2	84.5	86.3
<i>Masked Prediction:</i>						
SkeletonMAE [47]	Single-stream	STTFormer	86.6	92.9	76.8	79.1
SkeletonMAE [48]	Single-stream	STRRL	92.8	<u>96.5</u>	84.8	85.7
MAMP [31]	Single-stream	Transformer	93.1	97.5	<u>90.0</u>	<u>91.3</u>
MaskCLR [2]	Single-stream	Transformer	93.5	97.5	90.5	91.9
<i>Masked Prediction + Contrastive Learning:</i>						
W/o pre-training	Single-stream	Transformer	83.1	92.6	76.8	79.7
STARS-3stage (Ours)	Single-stream	Transformer	<u>93.2</u>	97.5	89.8	<u>91.3</u>
STARS (Ours)	Single-stream	Transformer	93.0	97.5	89.9	91.4

Table 3. Performance comparison on NTU-60 and NTU-120 in terms of the fine-tuning protocol. The best and second-best accuracies are in bold and underlined, respectively. * TF stands for Transformer.

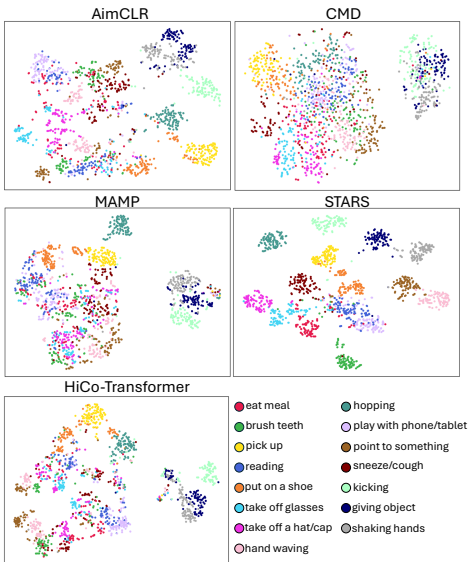


Figure 3. The t-SNE visualization of embedding features. We sample 15 action classes from the NTU-60 dataset and visualize the features extracted by our proposed STARS framework and compare it with AimCLR [18], CMD [30], HiCo-Transformer [10], and MAMP [31].

Method	To PKU-II		
	NTU 60	NTU 120	PKU-I
LongTGAN [54]	44.8	-	43.6
MS2L [26]	45.8	-	44.1
ISC [43]	51.1	52.3	45.1
CMD [30]	56.0	57.0	-
HaLP+CMD [37]	56.6	57.3	-
SkeletonMAE [47]	58.4	61.0	62.5
MAMP [31]	<u>70.6</u>	73.2	<u>67.8*</u>
STARS-3stage (Ours)	<u>71.8</u>	<u>72.7</u>	67.6
STARS (Ours)	71.9	72.2	68.5

Table 4. Performance comparison in the transfer learning protocol, where the source datasets are NTU-60 and NTU-120, and the target dataset is PKU-II. * indicates that result is reproduced using our GPUs.

not need negative samples for contrast and employs centring and sharpening techniques to prevent collapse. MoCo [19] is predominantly used by other contrastive learning approaches in action recognition [18, 25, 27]. It uses a memory bank to increase the negative samples in contrastive loss and a key encoder, which is updated via exponential moving average to maintain consistency. As shown in the Tab. 6, NNCLR significantly enhances KNN accuracy by forming

Method	1-shot	2-shot	5-shot
MAMP [31]	47.6	44.4	48.4
AimCLR [18]	48.9	45.9	51.1
HiCLR [52]	51.7	49.6	53.8
ISC [43]	55.4	53.3	57.1
HiCo-Transformer [10]	60.0	<u>58.2</u>	60.9
CMD [30]	<u>61.2</u>	<u>58.2</u>	61.3
STARS-3stage (Ours)	59.3	57.8	61.5
STARS (Ours)	63.5	62.2	65.7

Table 5. Performance comparison in the few-shot settings, where the model is pretrained on NTU-60 XSub and tested on 60 new samples of NTU-120 XSub.

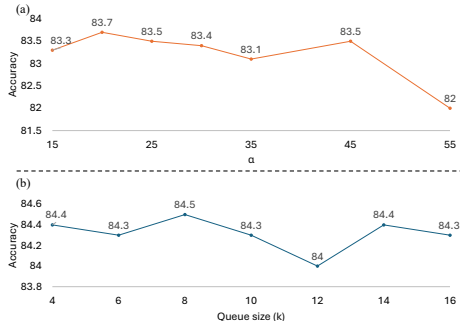


Figure 4. Ablation study on (a) layer-wise learning decay (b) Queue size. The performance is evaluated on the NTU-60 XSub dataset under the KNN evaluation protocol (K=10).

better clusters for different actions, while not using any data augmentations. For the remaining two strategies, we also examined the impact of including augmentation through spatial flipping and rotation. Generally, adding augmentations helps the methods achieve better performance; especially for MoCo, which relies on augmentations to construct the positive samples. Note that it is expected for the other two methods to further improve by incorporating more augmentations, which is not the focus of this study. Additional details about the hyperparameters in this ablation study are provided in the supplementary material.

Effect of Augmentation: Tab. 7 shows that applying augmentation results in a minor improvement in the KNN evaluation protocol. However, we chose not to use augmentation as our main method since the type of augmentation works heuristically and can result in different behavior in new scenarios, sometimes even degrading performance in cases such as shearing or axis masking. Additionally, we tested data augmentation on different evaluation protocols, such as linear evaluation, and did not observe any performance improvement.

Layer-wise Learning Rate Decay: As shown in Fig. 4 (a), we observe a decrease in accuracy with higher learning

Tuning Strategy	NTU-60	
	XSub	XView
DINO	77.6	86.3
DINO _{aug}	77.4	86.7
MoCo	72.2	86.7
MoCo _{aug}	73.9	88.0
NNCLR	81.9	89.6

Table 6. Ablation study on the tuning strategy. The performance is evaluated on the NTU-60 XSub and NTU-60 XView datasets under the KNN evaluation protocol (K=10).

Augmentation	NTU-60	
	XSub	XView
Spatial Flip	85.0	90.6
Rotation	84.8	90.1
Axis Mask	81.2	89.0
Shear	83.2	90.4
Spatial Flip + Rotation	84.6	90.4
No Augmentation	84.5	89.6

Table 7. Ablation study on the effect of augmentation. The performance is evaluated on the NTU-60 XSub and NTU-60 XView datasets under the KNN evaluation protocol (K=10).

decay. Our hypothesis is that increasing the decay causes the encoder to forget the robust representations learned in the initial stage, leading to performance degradation comparable to contrastive learning methods.

Queue size: Fig. 4 (b) explores how different queue sizes affect model accuracy during contrastive tuning, evaluated using the KNN protocol. The results indicate that the queue size has little impact on performance during pretraining. Based on these findings, we chose a queue size of 8k for all our evaluations.

5. Conclusion

In this work, we proposed a sequential contrastive tuning method. We find that masked prediction methods, despite showing promising results in various within-dataset evaluations, cannot outperform contrastive learning based methods in few-shot settings. By using our STARS framework, we show that we can further enhance the masked prediction baseline while achieving competitive results in few-shot settings, outperforming other models in 5-shot setting. However, when the dataset size is limited for pretraining, and for evaluations when encoder is fine-tuned with supervision, STARS cannot add significant value to its baseline.

References

- [1] Mohamed Abdelfattah and Alexandre Alahi. S-JEPA: A joint embedding predictive architecture for skeletal action recog-

nition. In *European Conference on Computer Vision*, pages 367–384. Springer, 2024.

[2] Mohamed Abdelfattah, Mariam Hassan, and Alexandre Alahi. MaskCLR: Attention-guided contrastive learning for robust action representation learning. In *Proceedings of the IEEE/CVF Conference on Computer Vision and Pattern Recognition*, pages 18678–18687, 2024.

[3] Mahmoud Assran, Mathilde Caron, Ishan Misra, Piotr Bojanowski, Florian Bordes, Pascal Vincent, Armand Joulin, Mike Rabbat, and Nicolas Ballas. Masked siamese networks for label-efficient learning. In *European Conference on Computer Vision*, pages 456–473. Springer, 2022.

[4] Hangbo Bao, Li Dong, Songhao Piao, and Furu Wei. BEiT: Bert pre-training of image transformers. *arXiv preprint arXiv:2106.08254*, 2021.

[5] Mathilde Caron, Ishan Misra, Julien Mairal, Priya Goyal, Piotr Bojanowski, and Armand Joulin. Unsupervised learning of visual features by contrasting cluster assignments. *Advances in neural information processing systems*, 33:9912–9924, 2020.

[6] Mathilde Caron, Hugo Touvron, Ishan Misra, Hervé Jégou, Julien Mairal, Piotr Bojanowski, and Armand Joulin. Emerging properties in self-supervised vision transformers. In *Proceedings of the IEEE/CVF international conference on computer vision*, pages 9650–9660, 2021.

[7] Yuxin Chen, Ziqi Zhang, Chunfeng Yuan, Bing Li, Ying Deng, and Weiming Hu. Channel-wise topology refinement graph convolution for skeleton-based action recognition. In *Proceedings of the IEEE/CVF international conference on computer vision*, pages 13359–13368, 2021.

[8] Yuxiao Chen, Long Zhao, Jianbo Yuan, Yu Tian, Zhaoyang Xia, Shijie Geng, Ligong Han, and Dimitris N Metaxas. Hierarchically self-supervised transformer for human skeleton representation learning. In *European Conference on Computer Vision*, pages 185–202. Springer, 2022.

[9] Kevin Clark, Minh-Thang Luong, Quoc V Le, and Christopher D Manning. ELECTRA: Pre-training text encoders as discriminators rather than generators. *arXiv preprint arXiv:2003.10555*, 2020.

[10] Jianfeng Dong, Shengkai Sun, Zhonglin Liu, Shujie Chen, Baolong Liu, and Xun Wang. Hierarchical contrast for unsupervised skeleton-based action representation learning. In *Proceedings of the AAAI Conference on Artificial Intelligence*, pages 525–533, 2023.

[11] Alexey Dosovitskiy, Lucas Beyer, Alexander Kolesnikov, Dirk Weissenborn, Xiaohua Zhai, Thomas Unterthiner, Mostafa Dehghani, Matthias Minderer, Georg Heigold, Sylvain Gelly, et al. An image is worth 16x16 words: Transformers for image recognition at scale. *arXiv preprint arXiv:2010.11929*, 2020.

[12] Haodong Duan, Jiaqi Wang, Kai Chen, and Dahua Lin. DG-STGCN: dynamic spatial-temporal modeling for skeleton-based action recognition. *arXiv preprint arXiv:2210.05895*, 2022.

[13] Haodong Duan, Jiaqi Wang, Kai Chen, and Dahua Lin. PYISK: Towards good practices for skeleton action recognition. In *Proceedings of the 30th ACM International Conference on Multimedia*, pages 7351–7354, 2022.

[14] Debidatta Dwibedi, Yusuf Aytar, Jonathan Tompson, Pierre Sermanet, and Andrew Zisserman. With a little help from my friends: Nearest-neighbor contrastive learning of visual representations. In *Proceedings of the IEEE/CVF International Conference on Computer Vision*, pages 9588–9597, 2021.

[15] Luca Franco, Paolo Mandica, Bharti Munjal, and Fabio Galasso. Hyperbolic self-paced learning for self-supervised skeleton-based action representations. *arXiv preprint arXiv:2303.06242*, 2023.

[16] Robert Geirhos, Jörn-Henrik Jacobsen, Claudio Michaelis, Richard Zemel, Wieland Brendel, Matthias Bethge, and Felix A Wichmann. Shortcut learning in deep neural networks. *Nature Machine Intelligence*, 2(11):665–673, 2020.

[17] Jean-Bastien Grill, Florian Strub, Florent Altché, Corentin Tallec, Pierre Richemond, Elena Buchatskaya, Carl Doersch, Bernardo Avila Pires, Zhaohan Guo, Mohammad Gheshlaghi Azar, et al. Bootstrap your own latent-a new approach to self-supervised learning. *Advances in neural information processing systems*, 33:21271–21284, 2020.

[18] Tianyu Guo, Hong Liu, Zhan Chen, Mengyuan Liu, Tao Wang, and Runwei Ding. Contrastive learning from extremely augmented skeleton sequences for self-supervised action recognition. In *Proceedings of the AAAI Conference on Artificial Intelligence*, pages 762–770, 2022.

[19] Kaiming He, Haoqi Fan, Yuxin Wu, Saining Xie, and Ross Girshick. Momentum contrast for unsupervised visual representation learning. In *Proceedings of the IEEE/CVF conference on computer vision and pattern recognition*, pages 9729–9738, 2020.

[20] Yilei Hua, Wenhan Wu, Ce Zheng, Aidong Lu, Mengyuan Liu, Chen Chen, and Shiqian Wu. Part aware contrastive learning for self-supervised action recognition. *arXiv preprint arXiv:2305.00666*, 2023.

[21] Sergey Ioffe and Christian Szegedy. Batch normalization: Accelerating deep network training by reducing internal covariate shift. In *International conference on machine learning*, pages 448–456. pmlr, 2015.

[22] Evangelos Kazakos, Arsha Nagrani, Andrew Zisserman, and Dima Damen. EPIC-fusion: Audio-visual temporal binding for egocentric action recognition. In *Proceedings of the IEEE/CVF International Conference on Computer Vision*, pages 5492–5501, 2019.

[23] Jungho Lee, Minhyeok Lee, Dogyoon Lee, and Sangyoun Lee. Hierarchically decomposed graph convolutional networks for skeleton-based action recognition. In *Proceedings of the IEEE/CVF International Conference on Computer Vision*, pages 10444–10453, 2023.

[24] Johannes Lehner, Benedikt Alkin, Andreas Fürst, Elisabeth Rumetshofer, Lukas Miklautz, and Sepp Hochreiter. Contrastive tuning: A little help to make masked autoencoders forget. *arXiv preprint arXiv:2304.10520*, 2023.

[25] Linguo Li, Minsi Wang, Bingbing Ni, Hang Wang, Jiancheng Yang, and Wenjun Zhang. 3d human action representation learning via cross-view consistency pursuit. In *Proceedings of the IEEE/CVF conference on computer vision and pattern recognition*, pages 4741–4750, 2021.

[26] Lilang Lin, Sijie Song, Wenhan Yang, and Jiaying Liu. MS²L: Multi-task self-supervised learning for skeleton

based action recognition. In *Proceedings of the 28th ACM International Conference on Multimedia*, pages 2490–2498, 2020.

[27] Lilang Lin, Jiahang Zhang, and Jiaying Liu. Actionlet-dependent contrastive learning for unsupervised skeleton-based action recognition. In *Proceedings of the IEEE/CVF Conference on Computer Vision and Pattern Recognition*, pages 2363–2372, 2023.

[28] Chunhui Liu, Yueyu Hu, Yanghao Li, Sijie Song, and Jiaying Liu. PKU-MMD: A large scale benchmark for continuous multi-modal human action understanding. *arXiv preprint arXiv:1703.07475*, 2017.

[29] Jun Liu, Amir Shahroudy, Mauricio Perez, Gang Wang, Ling-Yu Duan, and Alex C Kot. NTU RGB+D 120: A large-scale benchmark for 3d human activity understanding. *IEEE transactions on pattern analysis and machine intelligence*, 42(10):2684–2701, 2019.

[30] Yunyao Mao, Wengang Zhou, Zhenbo Lu, Jiajun Deng, and Houqiang Li. CMD: Self-supervised 3d action representation learning with cross-modal mutual distillation. In *European Conference on Computer Vision*, pages 734–752. Springer, 2022.

[31] Yunyao Mao, Jiajun Deng, Wengang Zhou, Yao Fang, Wanli Ouyang, and Houqiang Li. Masked motion predictors are strong 3d action representation learners. In *Proceedings of the IEEE/CVF International Conference on Computer Vision (ICCV)*, 2023.

[32] Yunyao Mao, Jiajun Deng, Wengang Zhou, Zhenbo Lu, Wanli Ouyang, and Houqiang Li. \mathbb{I}^2 MD: 3d action representation learning with inter-and intra-modal mutual distillation. *arXiv preprint arXiv:2310.15568*, 2023.

[33] Shlok Mishra, Joshua Robinson, Huiwen Chang, David Jacobs, Aaron Sarna, Aaron Maschinot, and Dilip Krishnan. A simple, efficient and scalable contrastive masked autoencoder for learning visual representations. *arXiv preprint arXiv:2210.16870*, 2022.

[34] Ashish S Nikam and Aarti G Ambekar. Sign language recognition using image based hand gesture recognition techniques. In *2016 online international conference on green engineering and technologies (IC-GET)*, pages 1–5. IEEE, 2016.

[35] Namuk Park, Wonjae Kim, Byeongho Heo, Taekyung Kim, and Sangdoo Yun. What do self-supervised vision transformers learn? *arXiv preprint arXiv:2305.00729*, 2023.

[36] Alexandre Sablayrolles, Matthijs Douze, Cordelia Schmid, and Hervé Jégou. Spreading vectors for similarity search. *arXiv preprint arXiv:1806.03198*, 2018.

[37] Anshul Shah, Aniket Roy, Ketul Shah, Shlok Mishra, David Jacobs, Anoop Cherian, and Rama Chellappa. HaLP: Hallucinating latent positives for skeleton-based self-supervised learning of actions. In *Proceedings of the IEEE/CVF Conference on Computer Vision and Pattern Recognition*, pages 18846–18856, 2023.

[38] Amir Shahroudy, Jun Liu, Tian-Tsong Ng, and Gang Wang. BTU RGB+D: A large scale dataset for 3d human activity analysis. In *Proceedings of the IEEE conference on computer vision and pattern recognition*, pages 1010–1019, 2016.

[39] Chenyang Si, Xuecheng Nie, Wei Wang, Liang Wang, Tie-niu Tan, and Jiashi Feng. Adversarial self-supervised learning for semi-supervised 3d action recognition. In *Computer Vision–ECCV 2020: 16th European Conference, Glasgow, UK, August 23–28, 2020, Proceedings, Part VII 16*, pages 35–51. Springer, 2020.

[40] Kun Su, Xiulong Liu, and Eli Shlizerman. PREDICT & CLUSTER: Unsupervised skeleton based action recognition. In *Proceedings of the IEEE/CVF Conference on Computer Vision and Pattern Recognition*, pages 9631–9640, 2020.

[41] Shengkai Sun, Daizong Liu, Jianfeng Dong, Xiaoye Qu, Junyu Gao, Xun Yang, Xun Wang, and Meng Wang. Unified multi-modal unsupervised representation learning for skeleton-based action understanding. In *Proceedings of the 31st ACM International Conference on Multimedia*, pages 2973–2984, 2023.

[42] Chenxin Tao, Xizhou Zhu, Weijie Su, Gao Huang, Bin Li, Jie Zhou, Yu Qiao, Xiaogang Wang, and Jifeng Dai. Siamese image modeling for self-supervised vision representation learning. In *Proceedings of the IEEE/CVF Conference on Computer Vision and Pattern Recognition*, pages 2132–2141, 2023.

[43] Fida Mohammad Thoker, Hazel Doughty, and Cees GM Snoek. Skeleton-contrastive 3d action representation learning. In *Proceedings of the 29th ACM international conference on multimedia*, pages 1655–1663, 2021.

[44] Yonglong Tian, Chen Sun, Ben Poole, Dilip Krishnan, Cordelia Schmid, and Phillip Isola. What makes for good views for contrastive learning? *Advances in neural information processing systems*, 33:6827–6839, 2020.

[45] Luya Wang, Feng Liang, Yangguang Li, Honggang Zhang, Wanli Ouyang, and Jing Shao. RePre: Improving self-supervised vision transformer with reconstructive pre-training. *arXiv preprint arXiv:2201.06857*, 2022.

[46] Shih-En Wei, Nick C Tang, Yen-Yu Lin, Ming-Fang Weng, and Hong-Yuan Mark Liao. Skeleton-augmented human action understanding by learning with progressively refined data. In *Proceedings of the 1st ACM International Workshop on Human Centered Event Understanding from Multimedia*, pages 7–10, 2014.

[47] Wenhan Wu, Yilei Hua, Ce Zheng, Shiqian Wu, Chen Chen, and Aidong Lu. SkeletonMAE: Spatial-temporal masked autoencoders for self-supervised skeleton action recognition. In *2023 IEEE International Conference on Multimedia and Expo Workshops (ICMEW)*, pages 224–229. IEEE, 2023.

[48] Hong Yan, Yang Liu, Yushen Wei, Zhen Li, Guanbin Li, and Liang Lin. SkeltonMAE: graph-based masked autoencoder for skeleton sequence pre-training. In *ICCV*, pages 5606–5618, 2023.

[49] LI Yang, Jin Huang, TIAN Feng, WANG Hong-An, and DAI Guo-Zhong. Gesture interaction in virtual reality. *Virtual Reality & Intelligent Hardware*, 1(1):84–112, 2019.

[50] Siyuan Yang, Jun Liu, Shijian Lu, Meng Hwa Er, and Alex C Kot. Skeleton cloud colorization for unsupervised 3d action representation learning. In *Proceedings of the IEEE/CVF International Conference on Computer Vision*, pages 13423–13433, 2021.

- [51] Haoyuan Zhang, Yonghong Hou, Wenjing Zhang, and Wanqing Li. Contrastive positive mining for unsupervised 3d action representation learning. In *European Conference on Computer Vision*, pages 36–51. Springer, 2022.
- [52] Jiahang Zhang, Lilang Lin, and Jiaying Liu. Hierarchical consistent contrastive learning for skeleton-based action recognition with growing augmentations. In *Proceedings of the AAAI Conference on Artificial Intelligence*, pages 3427–3435, 2023.
- [53] Jiahang Zhang, Lilang Lin, and Jiaying Liu. Prompted contrast with masked motion modeling: Towards versatile 3d action representation learning. In *Proceedings of the 31st ACM International Conference on Multimedia*, pages 7175–7183, 2023.
- [54] Nenggan Zheng, Jun Wen, Risheng Liu, Liangqu Long, Jianhua Dai, and Zhefeng Gong. Unsupervised representation learning with long-term dynamics for skeleton based action recognition. In *Proceedings of the AAAI Conference on Artificial Intelligence*, 2018.
- [55] Jinghao Zhou, Chen Wei, Huiyu Wang, Wei Shen, Cihang Xie, Alan Yuille, and Tao Kong. iBOT: Image bert pre-training with online tokenizer. *arXiv preprint arXiv:2111.07832*, 2021.
- [56] Yujie Zhou, Haodong Duan, Anyi Rao, Bing Su, and Jiaqi Wang. Self-supervised action representation learning from partial spatio-temporal skeleton sequences. *arXiv preprint arXiv:2302.09018*, 2023.
- [57] Wentao Zhu, Xiaoxuan Ma, Zhaoyang Liu, Libin Liu, Wayne Wu, and Yizhou Wang. MotionBERT: A unified perspective on learning human motion representations. In *Proceedings of the IEEE/CVF International Conference on Computer Vision*, pages 15085–15099, 2023.

STARS: Self-supervised Tuning for 3D Action Recognition in Skeleton Sequences

Supplementary Material

A. 3-Stage Design

An alternative pretraining method is to follow MAE-CT [24] and tune the encoder in 3 stages. Figure 5 shows the 3-stage design. Initially, when we initialize the projector and predictor modules, we freeze the encoder weights. In the second stage, we exclusively train the projector and predictor modules until they can effectively differentiate between different sequences using the NNCLR approach. Finally, in the third stage, we fine-tune the encoder weights using layer-wise learning rate decay. One motivation for this staged approach is the idea that the NNCLR head’s random weights could interfere with the representation quality by mapping the features into a random space, disrupting the learned structure. However, our findings challenge this assumption. The t-SNE visualization in Fig. 6 demonstrates that even with random NNCLR head weights, the cluster structure in the encoder’s output space remains intact in the new representation space. Furthermore, we observed with STARS-3stage that replicating this three-stage process not only increases training time but also leads to a drop in final accuracy. As a result, we use a two-stage design in our proposed STARS method.

B. Semi-supervised Evaluation Results

In semi-supervised evaluation protocol, we follow previous works [25, 30, 31] and fine-tune the pretrained encoder in addition to a post-attached classifier while given a small fraction of the training dataset. Specifically, the performance on the NTU-60 is reported while using 1% and 10% of the training set. Since the training portions are selected randomly, we report the result averaged over 5 different runs as the final result. As shown in Tab. 8, STARS is more effective in all scenarios. Specifically, while using 1% of the training data, leading to an increase in accuracy for the MAMP baseline by 3.1% and 4.2% in cross-subject and cross-view evaluations, respectively.

C. Ablation Hyper-parameters

Tab. 9 shows the hyperparameters used in DINOTuning strategy. For simplicity and because of limitation in resources, we used only two global views and did not use any local views in DINO. As shown in Tab. 10, we can see that incorporating local views led to a small improvement in performance. However, it came at the cost of significantly more resources. To be specific, we introduced two local views that randomly trimmed a section of the sequence between 40% and 80% and fed it only to the student network.

Method	NTU-60			
	XSub (1%)	XSub (10%)	XView (1%)	XView (10%)
<i>Other pretext tasks:</i>				
LongT GAN [54]	35.2	62.0	-	-
ASSL [39]	-	64.3	-	69.8
<i>Contrastive Learning:</i>				
MS ² L [26]	33.1	65.1	-	-
ISC [43]	35.7	65.9	38.1	72.5
3s-CrossSCLR [25]	51.1	74.4	50.0	77.8
3s-Colorization [50]	48.3	71.7	52.5	78.9
CMD [30]	50.6	75.4	53.0	80.2
3s-Hi-TRS [8]	49.3	77.7	51.5	81.1
3s-AimCLR [18]	54.8	78.2	54.3	81.6
3s-CMD [30]	55.6	79.0	55.5	82.4
CPM [51]	56.7	73.0	57.5	77.1
<i>Masked Prediction:</i>				
SkeletonMAE [47]	54.4	80.6	54.6	83.5
MAMP [31]	66.0	88.0	68.7	91.5
<i>Masked Prediction + Contrastive Learning:</i>				
PCM ³ [53]	53.1	82.8	53.8	77.1
STARS-3stage (Ours)	68.6	88.2	72.5	91.8
STARS (Ours)	69.1	88.0	72.9	91.8

Table 8. Performance comparison on the NTU-60 dataset under the semi-supervised evaluation protocol, with the final performance reported as the average of five runs.

With these additional views, we had to reduce the batch size to 16 and double the training time. Consequently, in our other experiments, we stuck to using only global views. We also used Sinkhorn-Knopp centering [5] a KoLeo regularizer [36] to help the convergence. Tab 13 shows the hyperparameters used in MoCoTuning. Similar to previous approaches [18, 25], we used 32K as the queue size, 0.999 for the momentum and 0.07 for the temperature.

Method	10-NN	20-NN	40-NN
w/o local views	77.4	77.1	77.0
w/ local views	77.8	78.0	77.6

Table 10. Effect of including local views on DINOTuning.

C.1. Algorithm psuedo code

Algo. 1 demonstrates the process in PyTorch-style pseudo code.

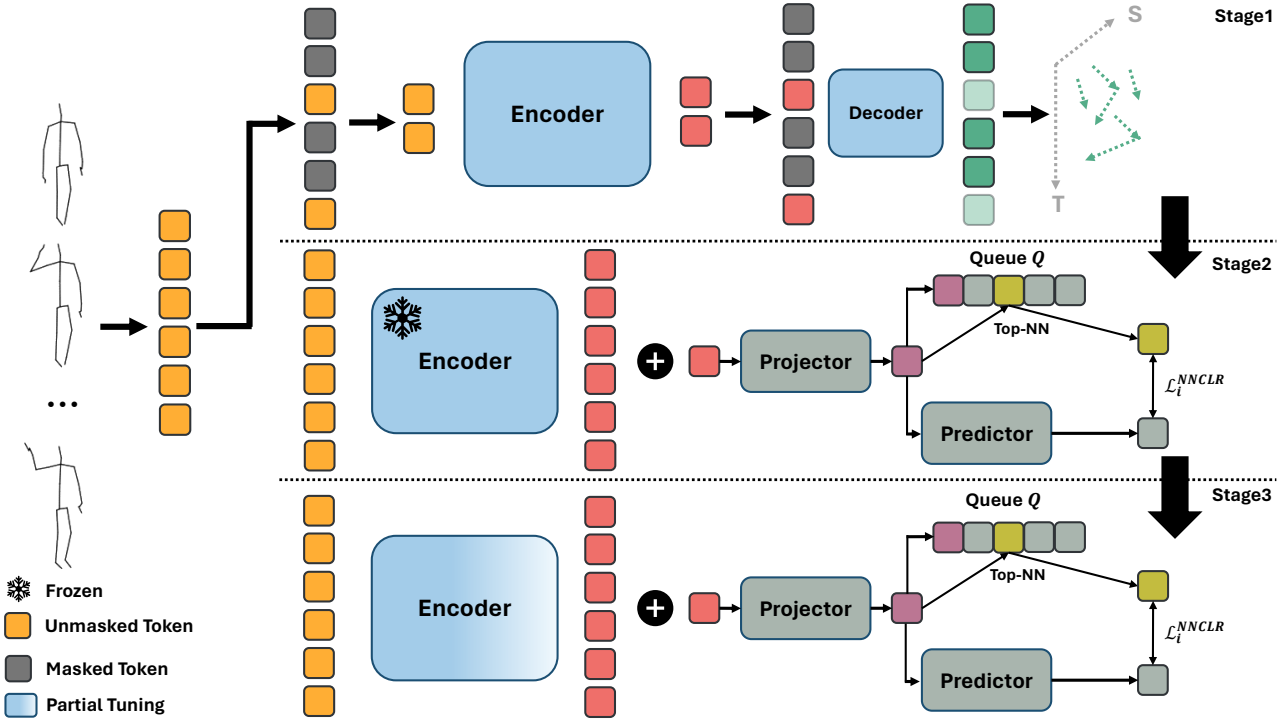


Figure 5. The overall pipeline of our proposed STARS-3stage framework. The first stage uses MAMP [31] to reconstruct the motion of masked tokens. The second stage keeps the encoder parameters frozen and trains parameters of the projector and predictor using a contrastive learning approach. After these parameters have converged to well-separated clusters, the third stage involves partial-tuning of the encoder parameters.

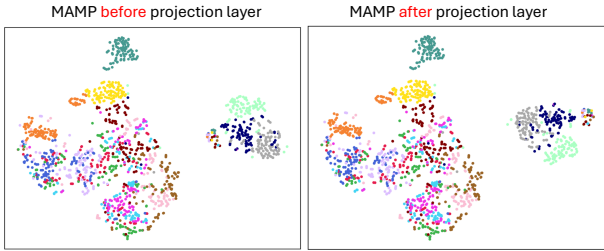


Figure 6. Comparison between MAMP’s output vectors before and after using a projection layer with random weights.

Hyperparameter	Value
Learning rate	0.001
Batch size	32
Augmentations	Mirroring & Rotation
Centering	Sinkhorn Knopp
KoLeo weight	0.1
# Global views	2
# Local views	0
Student temperature	0.1
Teacher temperature	0.04
Teacher momentum	0.996

Table 9. DINOTuning hyperparameters for ablation study in tuning strategy design.

D. Additional Ablation Studies

Combining MAMP and NNCLR.: One idea to tune the encoder in second stage is to combine NNCLR with MAMP and use both. Tab 11 compares this tuning stage with the proposed STARS. By including MAMP in the second stage of tuning, although it improves the final representation of encoder compared to the baseline (MAMP), it cannot perform as effective as STARS.

Training NNCLR from scratch: Table 12 presents the K-NN evaluation results for training the transformer from

scratch using the NNCLR method for 300 epochs. Without augmentation, the model struggles to select positive samples in contrastive learning that truly represent the same actions. This happens because the encoder starts with random weights, which lack meaningful cluster separation. Consequently, the encoder fails to fully use the advantages of NNCLR in the second stage of STARS, resulting in poorer performance.

Algorithm 1 PyTorch-style pseudo-code of contrastive tuning in the second stage.

```

1  # f: MAMP Encoder. Only second-half is tuned.
2  # g: Projector. Batch normalization module
3  # h: Predictor. 2 layer MLP, hidden size 4096,
4  # output 256
5  # Q: Queue with length of 32,768
6  for x in loader:
7      y = f(x) # encoder forward pass
8      z = g(y) # projection forward pass
9      p = h(z) # prediction forward pass
10     z, p = normalize(z, dim=1), normalize(p, dim=1)
11     nn = top_nn(z, Q) # finding nearest-neighbor
12         sample in Q
13     loss = L(nn, p)
14     loss.backward()
15     optimizer.step()
16     update_queue(Q, z)
17
18 def top_nn(z, Q):
19     similarities = z @ Q.T
20     idx = similarities.max(dim=1)
21     return Q[idx]
22
23 def L(nn, p, temperature=0.07):
24     logits = nn @ p.T
25     logits /= temperature # sharpening
26     labels = torch.arange(p.shape[0])
27     loss = cross_entropy(logits, labels)
28     return loss

```

Method	NTU-60	
	XSub	XView
MAMP (Baseline)	63.1	80.3
STARS	79.9	88.6
MAMP + NNCLR	74.6	86.5

Table 11. Ablation study on second stage of tuning. The performance is evaluated on the NTU-60 XSub and NTU-60 XView datasets under the KNN evaluation protocol (K=1).

K	NTU-60	
	XSub	XView
1	37.6	30.5
2	35.8	28.7
5	39.9	32.3
10	41.2	33.6

Table 12. Training the transformer encoder using NNCLR method from scratch. The performance is evaluated on the NTU-60 XSub and NTU-60 XView datasets under the KNN evaluation protocol.

Using naive MAE instead of MAMP: Tab. 14 and Tab.15 present a comparison of K-NN and few-shot evaluations for a variant that uses naive MAE instead of MAMP in the first stage. While tuning in the second stage leads to significant improvements, the overall performance remains lower because MAE performs worse than MAMP in the initial stage.

Effect of Batch Size. Table 16 reports the effect of varying the effective batch size on K-NN classification accuracy.

Hyperparameter	Value
Learning rate	0.001
Batch size	32
Augmentations	Mirroring & Rotation
Queue size	32,768
Momentum	0.999
Temperature	0.07

Table 13. MoCo hyperparameters for ablation study in tuning strategy design.

Method	NTU-60	
	XSub	XView
MAMP	63.1	80.3
STARS	79.9	88.6
MAE	44.1	43.7
STARS-MAE	53.5	55.2

Table 14. Ablation study on K-NN evaluation by changing the first-stage of STARS to naive MAE.

Method	1-shot	2-shot	5-shot
MAMP	47.6	44.4	48.4
STARS	63.5	62.2	65.7
MAE	35.0	31.8	34.2
STARS-MAE	41.5	37.9	40.6

Table 15. Ablation study on first few-shot evaluation by changing the first-stage of STARS to naive MAE.

Batch size	K-NN Acc. (%)
16	76.7
32	78.9
64	78.3
128	79.9

Table 16. Impact of effective batch size (i.e., number of negative samples) on K-NN accuracy, evaluated on NTU60-XSub. (K=1)

Increasing the batch size, which corresponds to sampling more negatives, generally improves accuracy, with the best performance observed at a batch size of 128. This highlights the importance of large negative sets for robust representation.

Setting	K-NN Acc. (%)
$\alpha = 1.0$	74.3
$\alpha = 0.2$	83.7

Table 17. Effect of tuning strength α on K-NN accuracy with $K = 10$, evaluated on NTU60-XSub.

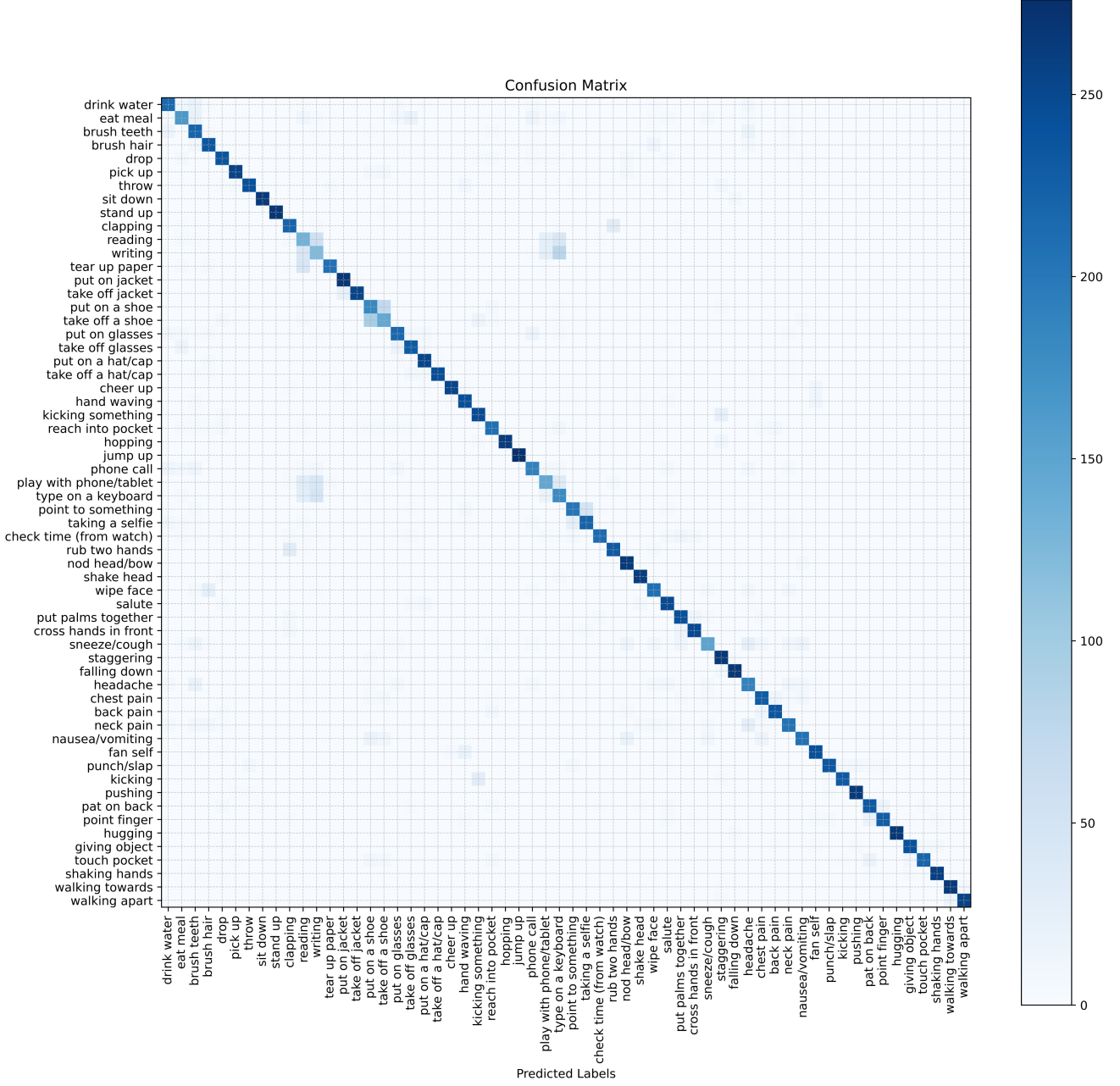


Figure 7. Confusion matrix of KNN evaluation in NTU-60 XSub dataset (k=10).

Effect of layer decay. As shown in Fig. 4 of the main paper, applying layer decay with $\alpha = 0.2$ yields the best performance. For comparison, we also evaluate the case of $\alpha = 1$, where all layers are tuned uniformly. Table 17 compares the effect of different tuning strengths on K -NN accuracy with $K = 10$. While full tuning ($\alpha = 1.0$) achieves moderate performance, reducing the tuning strength to $\alpha = 0.2$ substantially improves accuracy, suggesting that partial

tuning helps preserve more generalizable representations.

Method	Parameters (M)	MACs (G)
MAMP	10.34	250.4
STARS	8.43	606.1

Table 18. Comparison of model size and computational cost between MAMP and STARS.

Parameters and MACs. Tab. 18 shows that STARS requires fewer parameters than MAMP, as it employs an MLP-based decoder instead of a transformer decoder. However, its MACs are significantly higher because training involves two forward passes for the contrastive loss as well as the additional computation needed to identify nearest neighbors and apply the loss.

E. Confusion Matrix

Fig. 7 illustrates the confusion matrix under KNN evaluation protocol when K=10 on NTU-60 XSub dataset. The errors depicted in the figure can be classified into two distinct categories. Firstly, there are errors stemming from a lack of contextual information. For instance, when only a skeletal sequence is provided, actions like "play with phone/tablet" might be misinterpreted as "reading" and "writing." Secondly, there are errors arising from subtle movements, such as distinguishing between "clapping" and "hand rubbing," which pose challenges for the model in differentiation. In summary, these errors manifest due to either insufficient context or the intricacy of distinguishing minute actions, highlighting the complexities inherent in the task.